J. Fluid Mech. (2002), *vol.* 451, *pp.* 319–328.
DOI: 10.1017/S0022112001006954 Printed in the United Kingdom

Optimal perturbations in a four-vortex aircraft wake in counter-rotating configuration

By DAVID FABRE, LAURENT JACQUIN AND ANTOINE LOOF

ONERA, Department of Fundamental and Experimental Aerodynamics, 8, rue des Vertugadins, 92190 Meudon, France

(Received 27 September 2001 and in revised form 16 October 2001)

We consider the instability of two vortex pairs in a counter-rotating configuration. Such configurations model vortex wakes observed behind aircraft with inboard vortices produced at the inboard flap edges and at the tips of the horizontal tail. The instability potential is characterized by an optimal perturbation analysis. This extends the analysis of Fabre & Jacquin (2000) which was restricted to particular stationary configurations, and that of Crouch (1997) which considered co-rotating configurations. A complete mapping of the optimal perturbations is presented. The optimal perturbations grow faster than the Crow (1970) instability. However, they correspond to short-wavelength perturbations mainly affecting the weaker inboard vortices. A possible strategy which consists of forcing a long wavelength is then investigated. Application of both the optimal and the long-wave optimal perturbations to reduction of vortex wake danger is discussed.

1. Introduction

Instabilities growing faster than the Crow (1970) instability, which pertains to a single vortex pair, are sought in order to consider reducing aircraft separation on landing and take-off. It was recently recognized that such instabilities can occur in vortex systems composed of more than two vortices. Such configurations exist in the extended near field (within a few decades of wing spans) in the wake of aircraft when landing or taking off. Fast cooperative instabilities have been found in such wakes in laboratory experiments (Ortega & Savas 2001; Ortega, Bristol & Savas 2001) and in flight tests (Corsiglia & Dunham 1976). The present paper aims at providing a theoretical evaluation of the instability potential of a four-vortex configuration, which is the simplest model of such a multipolar wake. We hope to provide indications about possible strategies for designing wing planforms that favour faster decay of the wake. The four-vortex configuration is displayed in figure 1(*a*). The outboard vortices (labelled 1 and 4) are characterized by circulations Γ_1 and $\Gamma_4 = -\Gamma_1$, core radii a_1, and are initially separated by a distance b_1. The inboard vortices (labelled 2 and 3) are characterized by circulations Γ_2 and $\Gamma_3 = -\Gamma_2$, core radii a_2, and are initially separated by a distance b_2. The inboard vortices may be co-rotating with respect to the outboard ones ($\Gamma_2/\Gamma_1 > 0$), such as those produced at the outer flap edges, or counter-rotating ($\Gamma_2/\Gamma_1 < 0$), such as those generated by the inner flap edges, the horizontal tail and, perhaps, the fuselage. Donaldson & Bilanin (1975) considered the two-dimensional evolution of this configuration, and showed that the system is either periodic (with the vortices orbiting around the vorticity centroids) or divergent (with the two pairs

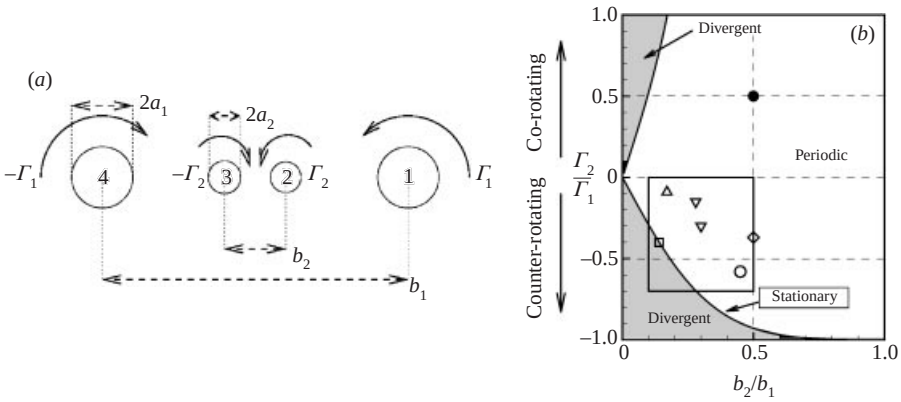

FIGURE 1. (*a*) Four-vortex wake model, and (*b*) classification chart. The symbols correspond to the theoretical and numerical studies of Crouch (1998) (●), Rennich & Lele (1999) and Fabre & Jacquin (2000) (□), and Quackenbush *et al.* (1997) (○), and to the experiments of Ortega *et al.* (2001) (◇), Jacquin *et al.* (2001) (△), and Coustols *et al.* (2001) (▽). The rectangular box corresponds to the region studied in the present work.

separating). They gave a classification chart (reproduced in figure 1*b*) of the periodic and divergent configurations versus the dimensionless parameters Γ_2/Γ_1 and b_2/b_1. The symbols in figure 1(*b*) refer to various studies. Crouch (1997) studied analytically a co-rotating configuration using Floquet theory. He identified two new instability mechanisms. The first is a short-wave instability, with a growth rate approximately twice that of the Crow instability. The second is a transient growth mechanism which mainly affects long wavelengths. Rennich & Lele (1999) computed the evolution of a wake leading to the formation of a four-vortex counter-rotating configuration. They showed that the presence of the inboard vortices strongly enhances the development of the Crow instability on the outboard vortices. They further showed that this effect is particularly strong if the vortices are close to particular configurations where they remain aligned. These stationary configurations correspond to the thick line in the lower part of figure 1(*b*). Fabre & Jacquin (2000) studied analytically the stability of these configurations. They showed that for long wavelengths, the growth rate of the instability is ten times higher than that of the Crow instability, in accordance with the computations of Rennich & Lele (1999). On the other hand, they showed that this long-wave instability is not the most amplified. The most amplified one is a short-wave instability which mainly affects the inboard vortices, and is expected to dissipate them without alteration of the outboard vortices. A long-wave instability should thus be forced in order to dissipate the outboard vortices. Other counter-rotating configurations in a different range of parameters have been studied numerically by Quackenbush *et al.* (1997), and experimentally by Ortega *et al.* (2001). In both studies, on each side of the wake, the inboard and outboard vortices undergo a rapidly growing Crow-type instability with a short wavelength, and at larger times vortex hoops form while the weaker inboard vortices wrap around the outboard vortices. Other symbols displayed in figure 1(*b*) correspond to experimental results for a small Airbus A300 model (Jacquin *et al.* 2001), and for a large transport aircraft of a type currently under study in the European research projects with two different flap configurations (Coustols *et al.* 2001). Note that in the Jacquin *et al.* (2001), two-point measurements revealed a significant correlation between the displacements of the inboard and outboard vortices, suggesting the existence of a cooperative instability mechanism.

The aim of this paper is to evaluate the instability potential of counter-rotating four-vortex configurations for a large range of parameters, represented by the rectangular box in figure 1(*b*). We use a linearized vortex filament method close to that used by Crouch (1997), (§ 2), and look for perturbations leading to an optimal growth at a fixed distance behind the aircraft (§ 3). This extends the study of Fabre & Jacquin (2000) to non-stationary configurations, and complements the work of Crouch (1997) who considered co-rotating configurations. As in Fabre & Jacquin (2000), two cases are considered. The first (§ 4) is the optimal perturbation which leads to a maximum growth of the instabilities. The second (§ 5), referred to as the 'long-wave optimal perturbation', corresponds to the symmetrical initial condition with a wavelength corresponding to that of the Crow instability which leads to a maximum amplification of the instabilities on the outboard vortices. Conclusions are given in § 6.

2. The linearized vortex filament method

The optimal perturbations are computed using a linearized vortex filament method identical to that in Crouch (1997), except that the self-induction terms are evaluated with the method proposed by Fabre & Jacquin (2000). The parametric equation for each of the four vortices is

$$\boldsymbol{X}_n(x,t) = [x,\, Y_n(t) + \hat{y}_n(t)\,\mathrm{e}^{\mathrm{i}kx},\, Z_n(t) + \hat{z}_n(t)\,\mathrm{e}^{\mathrm{i}kx}]. \tag{2.1}$$

Here Y_n and Z_n are the mean positions of the vortices, and $\hat{y}_n$ and $\hat{z}_n$ are the amplitudes (assumed small) of a three-dimensional perturbation with wavelength $\lambda = 2\pi/k$. The displacement velocities of the vortices are computed using the Biot–Savart law (except for the self-induction terms, see below). This gives, at leading order,

$$\frac{\mathrm{d}Y_n}{\mathrm{d}t} = \sum_{m\neq n} \frac{\Gamma_m Z_{mn}}{2\pi R_{mn}^2}, \quad \frac{\mathrm{d}Z_n}{\mathrm{d}t} = -\sum_{m\neq n} \frac{\Gamma_m Y_{mn}}{2\pi R_{mn}^2}. \tag{2.2a,b}$$

We use the simplifying notation $Y_{mn} = Y_m - Y_n$, $Z_{mn} = Z_m - Z_n$, and $R_{mn} = (Y_{mn}^2 + Z_{mn}^2)^{1/2}$. The initial conditions for (2.2*a*, *b*) are $Y_1(t_0) = b_1/2$, $Y_2(t_0) = b_2/2$, $Y_3(t_0) = -b_2/2$, $Y_4(t_0) = -b_1/2$ and $Z_1(t_0) = Z_2(t_0) = Z_3(t_0) = Z_4(t_0) = 0$, as described in figure 1(*a*). The set of equations governing the perturbation amplitudes is obtained at the following order in the linearization:

$$\begin{aligned}\frac{\mathrm{d}\hat{y}n}{\mathrm{d}t} &= \frac{\Gamma_n}{2\pi a_n^2}\varpi(ka_n)\hat{z}_n + \sum_{m\neq n}\frac{\Gamma_m Y_{mn} Z_{mn}}{\pi R_{mn}^4}(\hat{y}_n - \phi(kR_{mn})\hat{y}_m) \\ &\quad - \sum_{m\neq n}\frac{\Gamma_m}{2\pi R_{mn}^2}\left[\left(1 - \frac{2Z_{mn}^2}{R_{mn}^2}\right)\hat{z}_n - \left(\psi(kR_{mn}) - \frac{2Z_{mn}^2}{R_{mn}^2}\phi(kR_{mn})\right)\hat{z}_m\right], \end{aligned} \tag{2.3a}$$

$$\begin{aligned}\frac{\mathrm{d}\hat{z}_n}{\mathrm{d}t} &= -\frac{\Gamma_n}{2\pi a_n^2}\varpi(ka_n)\hat{z}_n - \sum_{m\neq n}\frac{\Gamma_m Y_{mn} Z_{mn}}{\pi R_{mn}^4}(\hat{z}_n - \phi(kR_{mn})\hat{z}_m) \\ &\quad + \sum_{m\neq n}\frac{\Gamma_m}{2\pi R_{mn}^2}\left[\left(1 - \frac{2Z_{mn}^2}{R_{mn}^2}\right)\hat{y}_n - \left(\psi(kR_{mn}) - \frac{2Z_{mn}^2}{R_{mn}^2}\phi(kR_{mn})\right)\hat{y}_m\right]. \end{aligned} \tag{2.3b}$$

Here a_n denotes the 'effective core radius' of the vortex labelled n (see Widnall, Bliss & Zalay 1971; Fabre & Jacquin 2000). The function ϖ appearing in (2.3*a*, *b*) corresponds to the self-induction effect of the perturbed vortices. This term is evaluated, following the method proposed by Fabre & Jacquin (2000), as the non-dimensional

frequency of a Kelvin wave of a Rankine vortex. As discussed by Fabre & Jacquin (2000), in the long-wave limit ($ka_{1,2} \ll 1$), this method is equivalent to the cutoff method used by Crouch (1997), and it applies regardless of the exact structure of the vortex cores. Moreover, this method does not lead to the prediction of short-wavelength spurious instabilities, contrary to the cutoff method. The functions ϕ and ψ characterize the mutual induction of the vortices. These functions involve the modified Bessel functions of second kind:

$$\psi(\beta) = \beta^2 K_0(|\beta|) + |\beta| K_1(|\beta|), \quad \phi(\beta) = \tfrac{1}{2}\beta^2 K_2(|\beta|). \tag{2.4}$$

The set of equations (2.3a, b) for the amplitudes of the three-dimensional perturbations is a linear, non-autonomous system, which can be written in the symbolic form

$$\frac{\mathrm{d}}{\mathrm{d}t}\boldsymbol{X}(t) = \boldsymbol{L}(t)\boldsymbol{X}(t), \tag{2.5}$$

where $\boldsymbol{X}(t) = (\hat{y}_1(t), \hat{z}_1(t), \hat{y}_2(t), \hat{z}_2(t), \hat{y}_3(t), \hat{z}_3(t), \hat{y}_4(t), \hat{z}_4(t))$ is a vector representing the perturbation amplitudes and $\boldsymbol{L}(t)$ is a 8×8 matrix containing the different terms of (2.3a, b). Using the generalized stability theory of Farell & Ioannou (1996), the general solution of this system can be written in the form

$$\boldsymbol{X}(t) = \boldsymbol{P}_{[t_0,t]}\boldsymbol{X}(t_0), \tag{2.6}$$

where $\boldsymbol{P}_{[t_0,t]}$ is the *propagator* of the system. This propagator is the 8×8 matrix which is the solution of the differential equation

$$\frac{\mathrm{d}}{\mathrm{d}t}\boldsymbol{P}_{[t_0,t]} = \boldsymbol{L}(t)\boldsymbol{P}_{[t_0,t]}, \tag{2.7}$$

with the initial condition $\boldsymbol{P}_{[t_0,t_0]} = \boldsymbol{I}$. Note that in the stationary cases the linear system (2.5) becomes autonomous and the propagator can be computed analytically as the exponential of the matrix $\boldsymbol{L}$, as done by Fabre & Jacquin (2000).

3. The optimal perturbations: definition

In order to characterize the instability potential, we define the 'optimal growth' G^{opt} as the maximum growth over all wavenumbers and all possible initial conditions, i.e.

$$G^{opt} = \max_k \max_{\|\boldsymbol{X}(t_0)\|=1} \| \boldsymbol{X}(t) \| \equiv \max_k \| \boldsymbol{P}_{[t_0,t]} \| . \tag{3.1}$$

Here $\| \boldsymbol{X} \|$ is the (Euclidian) norm of the perturbation amplitude vector, and $\| \boldsymbol{P}_{[t_0,t]} \|$ is the norm of the propagator matrix. We also define the 'optimal wavenumber' k^{opt} and the 'optimal perturbation' $\boldsymbol{X}^{opt}$ as the wavenumber and initial condition corresponding to the maximum in (3.1).

The optimal growth depends upon five non-dimensional parameters, namely the ratios Γ_2/Γ_1, b_2/b_1, a_1/b_1 and a_2/b_1 and a non-dimensional time $\bar{t}$, defined as

$$\bar{t} = \frac{\Gamma_1}{2\pi b_0^2}(t - t_0). \tag{3.2}$$

In his study of periodic co-rotating configurations, Crouch (1997) computed maximum amplifications for a time interval corresponding to the rotation period. Here we wish to compute optimal growths at fixed downstream distance X from the generating aircraft. This allows us to consider periodic, divergent and stationary configurations with a unique method. Suppose that the vortices have been generated by an aircraft

with velocity U_0, geometric wing span b_0, lift coefficient C_L and aspect ratio AR. The lift L of the aircraft is (see Donaldson & Bilanin 1975)

$$L = \frac{C_L}{2AR}\rho U_0^2 b_0^2 = \rho U_0 \Gamma_1 b_1 \left(1 + \frac{\Gamma_2 b_2}{\Gamma_1 b_1}\right), \tag{3.3}$$

where ρ is the density of the air. As the instabilities are essentially convective (see Fabre, Cossu & Jacquin 2000; Fabre & Jacquin 2000), the spatial amplifications can be deduced from the temporal ones through the change of variables $X = U_0(t - t_0)$. Using (3.2) and (3.3), this change of variables leads to

$$\frac{X}{b_0} = \frac{4\pi AR}{C_L}\left(1 + \frac{\Gamma_2 b_2}{\Gamma_1 b_1}\right)\left(\frac{b_1}{b_0}\right)^3 \bar{t}. \tag{3.4}$$

In the computation of the optimal growths, we have integrated numerically (2.2a, b) and (2.7a, b) using a fourth-order Runge–Kutta scheme, and computed the norm $\| \boldsymbol{P}_{[t_0,t]} \|$ in (3.1) as the highest singular value of the matrix (see Farell & Ioannou 1996). The method also allows us to compute the optimal perturbation, which corresponds to the associated singular vector.

4. The optimal perturbations: results

Figure 2, the main result of our work, describes the optimal perturbations computed for a downstream distance $X/b_0 = 30$, for circulation and separation ratios in the ranges $-0.7 \leqslant \Gamma_2/\Gamma_1 \leqslant 0$ and $0.1 \leqslant b_2/b_1 \leqslant 0.5$. The lift coefficient and aspect ratio of the generating aircraft were chosen as $C_L = 1.5$, $AR = 7$, typical values of landing configurations. The parameter b_1/b_0 was set to $\pi/4$. This choice is obtained by assuming that the outboard vortices are formed through the roll-up of vorticity shed by an elliptically loaded wing, see Donaldson & Bilanin (1975). The vortex radii were chosen as $a_1 = 0.1b_1$, $a_2 = 0.05b_1$ as in Fabre & Jacquin (2000). Several results are given in figure 2. The thin lines display iso-levels of the optimal growths G^{opt}. The dashed lines give a classification of the optimal wavelengths. A distinction is made between long wavelengths (LW, $k^{opt}b_1 < 1$), medium wavelengths (MW, $1 < k^{opt}b_1 < 4$), short wavelengths (SW, $4 < k^{opt}b_1 < 8$) and ultra-short wavelengths (USW, $k^{opt}b_1 > 8$). The shaded and white areas indicate, respectively, symmetrical and antisymmetrical optimal perturbations. The thick line corresponds to the stationary configurations.

For the divergent configurations located to the left of the thick line, the instability potential is particularly high. The optimal growth is always larger than 10^{20} and the corresponding optimal perturbation is a symmetrical perturbation with an ultra-short wavelength. In this range, the inboard vortices quickly escape from the influence of the outboard ones and at $X/b_0 = 30$ they are no longer in their proximity. The leading instability mechanism is simply the Crow instability on the inboard vortices; the corresponding perturbation is located almost entirely on the inboard vortices, and hardly affects the outboard vortices. Note that, as the inboard vortices escape, the resulting circulation is higher. Thus these configurations are unattractive. For the stationary configurations (thick line), the optimal perturbations correspond to short-wave symmetrical instabilities. Their optimal growth is of order 10^8. For $\Gamma_2/\Gamma_1 = -0.4$ and $b_2/b_1 = 0.14$, our results give $G^{opt} = 7.7 \times 10^8$, $k^{opt}b_1 = 7.2$, in agreement with Fabre & Jacquin (2000). Consider, now, the periodic configurations located to the right of the thick line. In this region, although they are several orders of magnitude smaller

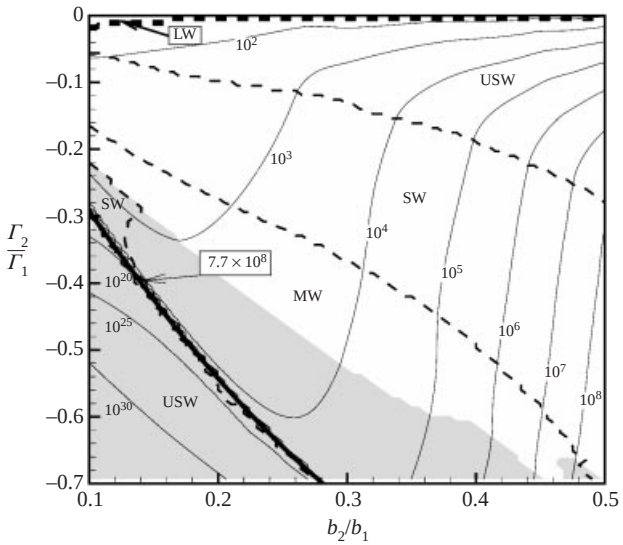

FIGURE 2. Optimal growth G^{opt} and properties of the optimal perturbations at $X/b_0 = 30$.

than for the divergent and stationary configurations, the optimal growths remain very high. Recall, for comparison, that in a single vortex pair the Crow instability grows only by a factor $\exp(0.8\bar{t}) \approx 2.2$ at $X/b_0 = 30$. The optimal perturbations are either symmetrical or antisymmetrical, and the optimal wavelengths range from medium to ultra-short. Note that a region of long wavelengths also exists, but it is limited to very weak inboard vortices ($|\Gamma_2/\Gamma_1| < 0.02$). In this range, the inboard vortices vanish and the optimal growth defined by (3.1), which takes into account the displacement of all of the vortices, is meaningless. Two regions of parameters are particularly interesting. The first is the region just to the right of the thick line, and corresponds to configurations which are nearly stationary. In this range, the optimal perturbations are symmetrical with medium or short wavelengths. The physical mechanism responsible for the strong amplifications is the strong interaction between the inboard vortices due to their proximity, as in Fabre & Jacquin (2000). However, this effect is felt in a very limited range of parameters, and the optimal growth decreases abruptly when moving away from the stationary case. The second interesting region is the lower right corner of figure 2, i.e. large b_2/b_1 and $|\Gamma_2/\Gamma_1|$. In this range, the optimal perturbations are antisymmetrical with short wavelengths. Here the physical mechanism was identified by Ortega *et al.* (2001) to be the generalized form of the Crow instability for the unequal vortex pairs of each half-plane.

Figure 3 displays, as an example, the optimal perturbation for $\Gamma_2/\Gamma_1 = -0.3$ and $b_2/b_1 = 0.3$, a case close to configurations that can be obtained in wind tunnel experiments using a representative aircraft model (Coustols *et al.* (2001)). For this configuration the location $X/b_0 = 30$ corresponds approximately to one period of rotation of the vortices. The corresponding optimal growth is $G^{opt} = 5677$ and the wavelength is $k^{opt}b_1 = 4.55$. The initial level of the perturbation is chosen arbitrarily at $\| \boldsymbol{X}(t_0) \| = 10^{-4}$. With this choice, the perturbations are not visible at $X/b_0 = 0$ and 10. They become visible at $X/b_0 = 20$, and reach a large magnitude at $X/b_0 = 30$. The figure shows that the optimal perturbation mainly affects the inboard vortices; in figure 3(*d*) the ratio of the displacement amplitudes of the outboard vortices to

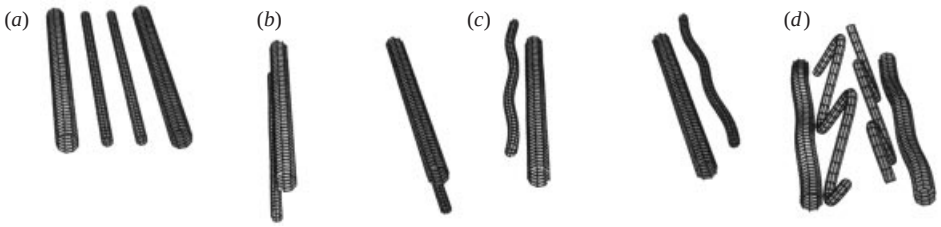

FIGURE 3. Optimal perturbation computed for $X/b_0 = 30$ in the case $\Gamma_2/\Gamma_1 = -0.3$, $b_2/b_1 = 0.3$. (*a*) $X/b_0 = 0$, (*b*) 10, (*c*) 20 and (*d*) 30.

that of the inboard vortices is about 7%. This ratio is always smaller than 10% for moderate values of $|\Gamma_2/\Gamma_1|$ ($\leqslant 0.35$).

Note that figure 3 qualitatively resembles the experimental vortex visualizations of Ortega *et al.* (2001), for $\Gamma_2/\Gamma_1 = -0.37$ and $b_2/b_1 = 0.5$. For this case, our results predict an optimal wavelength $k^{opt}b_1 \approx 7$ and an optimal growth $G^{opt} \approx 10^8$, which seems particularly favourable. Ortega *et al.* (2001) report a wavelength of $\lambda \approx b_1$ (thus $kb_1 \approx 2\pi$), and an antisymmetrical perturbation, in accordance with our results. They also show that the perturbations reach large amplitudes within 20–30 wing spans behind the wing, which confirms the high instability potential of this configuration.

We have also considered the dependence of the optimal growths upon the vortex radii $a_{1,2}$. In the whole range of parameters considered in figure 2, an increase of the vortex radii leads to a slight decrease of the optimal growth, and to a shift of the optimal wavelength toward short wavelengths.

5. The 'long-wave optimal' strategy

We have seen that the optimal perturbations can lead to very large growths. However, they poorly affect the outer vortices, at least in the linear régime. Whether these instabilities can effectively lead to a reduction of the wake vortex danger will depend upon the nonlinear régime. There are two different ways to reduce this danger (see Spalart 1998; Jacquin *et al.* 2001). The first is to reduce the overall circulation of the wake through transport of vorticity across the plane of symmetry of the wake. The second is to increase the dispersion of the vorticity. The optimal perturbations correspond to short wavelength, and, in many cases, to antisymmetric perturbations so they may not contribute to transport of vorticity across the plane of symmetry, but only to an increase of the vorticity dispersion. There is no guarantee that the subsequent nonlinear régime will not lead to a collapse to a new vortex pair, with the benefit of the linear instability being lost. Such a possibility suggests a different strategy. One strategy consists in promoting long-wave perturbations which will survive the nonlinear disruption of the inboard vortices and will keep on growing in the far field, leading finally to transport of vorticity through the plane of symmetry by the formation of vortex rings. This was the initial idea of Rennich & Lele (1999), also advocated by Fabre & Jacquin (2000). The instability potential of this strategy is evaluated in this section.

We set the wavelength to $k\tilde{b} = 0.8$, as in Rennich & Lele (1999). Here $\tilde{b}$ is the 'effective span' of the four-vortex system, defined as $(\Gamma_1 + \Gamma_2)\tilde{b} = \Gamma_1 b_1 + \Gamma_2 b_2$. This effective span is expected to correspond to the span of the resulting vortex pair after merging of the inboard and outboard vortices, see Rennich & Lele (1999). We define

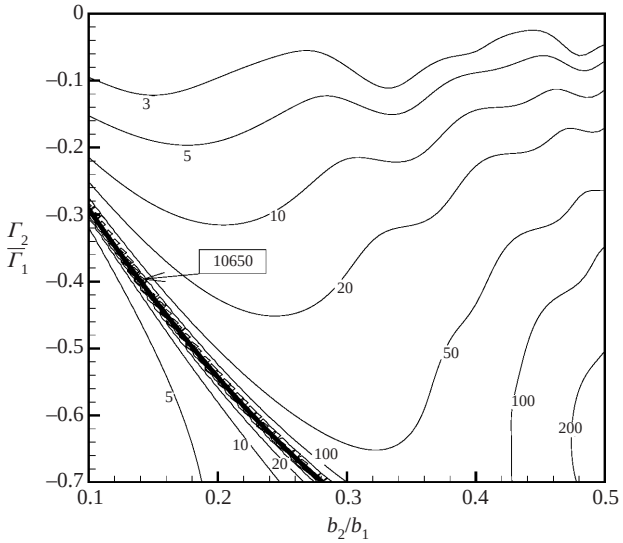

FIGURE 4. 'Long-wave optimal growth' G^{LW} computed for $X/b_0 = 30$.

the 'long-wave optimal growth' as

$$G^{LW} = \max_{\boldsymbol{X}(t_0)\in\mathscr{S},\|\boldsymbol{X}(t_0)\|=1,k\tilde{b}=0.8} \| X(t) \|_{out}. \tag{5.1}$$

Here $\mathscr{S}$ is the subspace of the symmetrical initial conditions, and $\| \boldsymbol{X} \|_{out} = (\hat{y}_1^2 + \hat{z}_1^2 + \hat{y}_4^2 + \hat{z}_4^2)^{1/2}$ is the norm of the perturbations on the outboard vortices only. This long-wave optimal growth is computed as the largest singular value of the 4×4 matrix, deduced from the propagator $\boldsymbol{P}_{[t_0,t]}$, which maps the symmetrical initial conditions to the corresponding final perturbations on the outer vortices. We also call the long-wave optimal perturbation the symmetrical initial condition $\boldsymbol{X}^{LW}$ corresponding to the maximum in (5.1).

Figure 4 displays iso-levels of the long-wave optimal growth at $X/b_0 = 30$ for the same parameters as in figure 2. Again, the growths obtained for the stationary configurations (thick line) are several orders of magnitude higher than for other configurations (for $\Gamma_2/\Gamma_1 = -0.4$, $b_2/b_1 = 0.14$, the value $G^{LW} = 10650$ is in accordance with the predictions of Fabre & Jacquin 2000). The periodic configurations with $\Gamma_2/\Gamma_1 < -0.3$ lead to long-wave optimal growth of order 10 or higher. As in figure 2, two regions of parameters are of a particular interest. The first is located just above the thick line corresponding to the stationary configurations, and the second is located in the lower right corner, with large b_2/b_1 and $|\Gamma_2/\Gamma_1|$. As in Fabre & Jacquin (2000), the long-wave stability properties are found to be weakly dependent upon the precise value of the vortex radii $a_{1,2}$. Note the wavy aspect of the contours for $G^{LW} = 3$, 5, 10 and 30. This is due to a transient effect during the vortex orbits (the number of rotation periods at $X/b_0 = 30$ predicted by (3.4) varies with the location in the figure).

For the case $\Gamma_2/\Gamma_1 = -0.3$, $b_2/b_1 = 0.3$ already considered, the growth at $X/b_0 = 30$ is $G^{LW} = 14.9$. This is almost 400 times smaller than the optimal growth ($G^{opt} = 5677$) but remains much higher than the growth of the Crow instability (which is close to 2.2). Figure 5 displays the long-wave optimal perturbation obtained for that case. The amplitude of the initial condition was chosen as $\| \boldsymbol{X}(t_0) \| = 2 \times 10^{-2}$. With this choice,

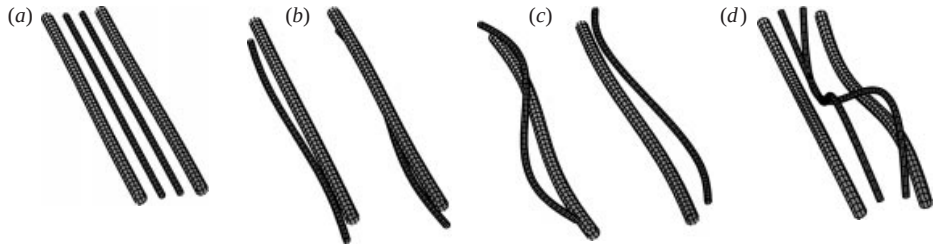

FIGURE 5. 'Long-wave optimal perturbation' computed for $X/b_0 = 30$ in the case $\Gamma_2/\Gamma_1 = -0.3$, $b_2/b_1 = 0.3$. (*a*) $X/b_0 = 0$, (*b*) 10, (*c*) 20, (*d*) 30.

the perturbation reaches a large magnitude at $X/b_0 = 30$. Note that the long-wave optimal perturbation favours the displacement of the outboard vortices: in figure 5(*d*) the ratio of outboard to inboard displacement amplitudes is 27% compared to 7% for the optimal perturbation in figure 3.

Note that the short-time behaviour of the long-wave optimal perturbation in figure 5 is similar to that of the perturbations leading to transient growth in co-rotating configurations (see figure 13 of Crouch 1997), with only a 180° phase shift to the weaker vortex perturbation (consistent with the sign change of the circulation ratio). On the other hand, the large-time behaviour is different: for co-rotation, after a rapid transient growth the perturbations rise at a slower rate corresponding to that of the Crow instability (see figure 12 of Crouch 1997), whereas for counter-rotation the perturbations continuously grow at a faster rate. For example, considering again the case $\Gamma_2/\Gamma_1 = -0.3$, $b_2/b_1 = 0.3$, amplifications as high as $G^{LW} = 137$ and 3046 are obtained, respectively, at $X/b_0 = 60$ and 100.

6. Summary and discussion

We have considered the instability properties of an aircraft wake model composed of two vortex pairs in a counter-rotating configuration, as obtained in the wake of aircrafts for particular wing planform configurations, with high levels of vorticity produced at the inner flap edges and at the tips of the horizontal tail. Note that other wing planforms may lead to co-rotating four-vortex configurations; the stability analysis of such configurations was conducted by Crouch (1997).

The counter-rotating configurations may be periodic, divergent or stationary. The present work extends to periodic and divergent configurations the stability analysis conducted by Fabre & Jacquin (2000) on stationary cases. We have characterized the instability potential of such vortex systems in two different ways. First, we considered optimal perturbations, which correspond to the perturbations leading to the largest amplifications over all wavenumbers. Secondly, we considered 'long-wave optimal perturbations', defined as the symmetrical perturbations leading to the largest amplification of the instabilities for a long wavelength, corresponding to that of the Crow instability. We computed the corresponding amplifications at a downstream distance of 30 spans behind the generating aircraft, assuming a typical landing configuration.

For divergent configurations, the optimal perturbations affect only the inboard vortices, and the long-wave optimal perturbations lead to limited growths. For periodic configurations, very large optimal growths may be reached. Values as high as 10^6 to 10^8 are found for large values of b_2/b_1 (> 0.4). But, according to (3.3), for large $|\Gamma_2/\Gamma_1|$ and b_2/b_1 the circulation Γ_1 of the outboard vortices and thus the loading

at the wing tips has to be increased significantly to maintain a constant lift of the wing. A realistic aircraft wing is unlikely to support such a load at its extremities. Values of b_2/b_1 around 0.3 are thought to be more realistic for conventional wing planforms, see Coustols *et al.* (2001). With this constraint, at 30 wing spans, the optimal growths range from 10^3 to 10^4 and the long-wave optimal growths range from 10 to 100. Thus, both cases can lead to a large-amplitude perturbation close behind the aircraft, but a larger initial amplitude is required for the long-wave optimal perturbation. Even larger amplifications are obtained farther away. As a comparison, for the case of a single vortex pair, an amplification of a factor 10 is reached at 100 spans behind the aircraft. For the co-rotating configurations considered by Crouch (1997), a growth of a factor 10 is reached at 30 spans for the long-wave transient growth mechanism, and at 45 spans for the short-wave instability mechanism.

The optimal perturbation analysis is relevant to the linear régime of development of the instabilities. Whether these instabilities can effectively lead to a reduction of the wake vortex danger will depend upon the subsequent nonlinear régime. Forcing the long waves in a four-vortex system gives a better guarantee of final dissipation of the wake by transport of vorticity through the plane of symmetry whatever the outcome of the nonlinear interaction between the two initial vortex pairs.

This work was partially conducted in the framework of C-WAKE project funded by the European Community under grant number G4RD-CT-1999-00141.

REFERENCES

Corsiglia, V. R. & Dunham, R. E. 1976 Aircraft wake-vortex minimization by use of flaps. In *Wake Vortex Minimization*, pp. 305–338. NASA SP-409.

Coustols, E., Dor, J.-B., Jacquin, L. & Moens, F. 2001 Experimental study of the near-field wake of a large transport aircraft with various flap settings. In preparation.

Crouch, J. D. 1997 Instability and transient growth for two trailing-vortex pairs. *J. Fluid Mech.* **350**, 311–330.

Crow, S. 1970 Stability theory for a pair of trailing vortices. *AIAA J.* **8**, 2172–2179.

Donaldson, C. & Bilanin, A. 1975 Vortex wakes of conventional aircraft. *Tech. Rep.* AG-204. AGARD.

Fabre, D., Cossu, C. & Jacquin, L. 2000 Spatio-temporal development of the long and short-wave vortex-pair instabilities. *Phys. Fluids* **12**, 1247–1250.

Fabre, D. & Jacquin, L. 2000 Stability of a four-vortex aircraft wake model. *Phys. Fluids* **12**, 2438–2443.

Farell, B. F. & Ioannou, P. J. 1996 Generalized stability theory. Part I: Autonomous operators. Part II: Non-autonomous operators. *J. Atmos. Sci.* **53**, 2025–2041.

Jacquin, L., Fabre, D., Geffroy, P. & Coustols, E. 2001 The properties of a transport aircraft wake in the extended nearfield: an experimental study. *AIAA Paper* 2001–1038.

Ortega, J. M., Bristol, R. L. & Savas, O. 2001 Experimental study of the instability of unequal strength counter-rotating vortex pairs. *Submitted to J. Fluid Mech.*

Ortega, J. & Savas, O. 2001 Rapidly growing instability mode in trailing multiple-vortex wakes. *AIAA J.* **39**, 750–754.

Quackenbush, T., Bilanin, A., Batcho, P., McKilipp, R. & Carpenter, B. 1997 Implementation of vortex wake control using SMA-actuated devices. *Proc. SPIE* **3044**, 134–146.

Rennich, S. C. & Lele, S. K. 1999 A method for accelerating the destruction of aircraft wake vortices. *J. Aircraft* **36**, 398–404.

Spalart, P. 1998 Airplane trailing vortices. *Annu. Rev. Fluid Mech.* **30**, 107–138.

Widnall, S. E., Bliss, D. & Zalay, A. 1971 Theoretical and experimental study of the stability of a vortex pair. In *Aircraft Wake Turbulence* (ed. J. H. Olsen, A. Goldburg & M. Rodgers). Plenum.